RSC Advances

PAPER

View Article Online
View Journal | View Issue

Check for updates

Cite this: *RSC Adv.*, 2024, **14**, 22035

Enhancing the antimicrobial activity of silver nanoparticles against pathogenic bacteria by using *Pelargonium sidoides* DC extract in microwave assisted green synthesis

Renata Pascoal Illanes Tormena, [a] Mac-Kedson Medeiros Salviano Santos, [a] Atailson Oliveira da Silva, [a] Felipe Mourthé Félix, [a] Juliano Alexandre Chaker, [a] Daniel Oliveira Freire, [b] Izabel Cristina Rodrigues da Silva, [b] Sergio Enrique Moya [c] and Marcelo Henrique Sousa *[a]

This study presents an optimized microwave-assisted method for the green synthesis of silver nanoparticles (AgNPs) using a root extract obtained from *Pelargonium sidoides* DC. The influence of temperature, reagent concentration, and irradiation time was systematically investigated to enhance synthesis yield. Characterization techniques including XRD, UV-vis, FTIR, XPS, and zetametry were employed to confirm the successful formation of nanoparticles with a metallic silver core (~17 nm) functionalized with organic molecules derived from the plant extract. The cytotoxicity of AgNPs was assessed using a cell viability assay, while the Minimum Inhibitory Concentration (MIC) of nanoformulation against pathogenic bacteria, including *Staphylococcus aureus*, *Escherichia coli*, *Pseudomonas aeruginosa*, and the carbapenem-resistant *Klebsiella pneumoniae* (KPC), was determined using the Broth microdilution method. The nanoformulation synthesized with *P. sidoides* extract exhibited a dose-dependent response, demonstrating superior antimicrobial efficacy compared to the pure plant extract in most cases. The MIC values ranged from 0.85 to 17.1 μg mL^{-1}, with particularly strong performance against the drug resistant KPC strain. The enhanced antimicrobial effect is attributed to the synergistic action of the metallic silver core and phytochemicals from *P. sidoides* on the surface of nanoparticles, which also contribute to notable colloidal stability of AgNPs at physiological pH levels.

Received 6th June 2024
Accepted 30th June 2024

DOI: 10.1039/d4ra04140b

rsc.li/rsc-advances

Open Access Article. Published on 12 July 2024. Downloaded on 12/9/2025 5:59:04 AM.
This article is licensed under a Creative Commons Attribution-NonCommercial 3.0 Unported Licence.

Introduction

One of the most widespread applications of silver nanoparticles (AgNPs) is based on their broad spectrum of antimicrobial activity and high efficiency against various microorganisms, even in low doses.[1] Among synthetic routes, green synthesis of AgNPs offers a simple and eco-friendly approach, typically achievable through the reaction of silver ions (Ag^+) and a biological material with reducing properties, in a one-step process that avoids the production of more toxic residues.[2]

It is a consensus among scientists that plant extracts – predominantly utilized as biological resources for performing green synthesis – act not only as reducing agents but also form a stabilizing layer on the surface of AgNPs with phytochemicals that play a crucial role in enhancing colloidal stability at physiological pH and, most importantly, increase the intrinsic antimicrobial activity of the Ag^0 nanocore.[3] Plant extracts that already exhibit specific antimicrobial properties have been employed to impart more specificity in applications for AgNPs synthesized through this route.[4]

In this context, extracts of *Pelargonium sidoides* (*P. sidoides*), a South African native plant belonging to the Geraniaceae family with known antimicrobial activity,[5] have been used for the treatment of acute and chronic infections of the respiratory tract and ear, nose and throat.[6] The main pharmacological effects of *P. sidoides*, which involves antimicrobial action and/or stimulation of the nonspecific immune system,[7] triggered by the action of phytochemicals present in the extracts, primarily polymeric proanthocyanidins (with gallocatechin and epigallocatechin moieties), highly oxygenated coumarins, flavonoids, phenolic compounds, benzopyranones and derivatives of gallic and hydroxycinnamic acids.[8] In particular, umckalin is a typical coumarin and the main group most likely responsible for the pharmacological action of *P. sidoides*.[9]

Therefore, we hypothesized that using *P. sidoides* extract to synthesize AgNPs can result in nanostructured antimicrobials

[a]*Green Nanotechnology Group, University of Brasilia, DF 72220-900, Brasilia, Brazil. E-mail: mhsousa@unb.br; mhsqui@gmail.com*

[b]*Graduate Program in Health Sciences and Technologies, Faculty of Ceilandia, University of Brasília, DF 72220-900, Brasilia, Brazil*

[c]*Soft Matter Nanotechnology Laboratory, CIC biomaGUNE, 20009, San Sebastian, Guip, Spain*

© 2024 The Author(s). Published by the Royal Society of Chemistry

Open Access Article. Published on 12 July 2024. Downloaded on 12/9/2025 5:59:04 AM. This article is licensed under a Creative Commons Attribution-NonCommercial 3.0 Unported Licence.

with specificity against specific microorganisms, profiting from the synergy between the nanodimensional metallic silver core and the cover layer of *P. sidoides phytochemicals* acquired during the green synthesis. There are very few reports in the literature regarding the use of *P. sidoides* with nanosilver obtained from green synthesis or in mixtures as antimicrobial agents. Kgatshe *et al.* employed the ethanolic extract of *P. sidoides* for the synthesis of biogenic AgNPs.[10] Those researchers noted that AgNPs exhibit increased antimicrobial activity compared to the plant extract and demonstrated efficacy of the formulation against Gram-positive *Streptococcus pneumoniae* and *Bacillus cereus*, as well as Gram-negative *Moraxella catarrhalis*, *Escherichia coli*, and *Pseudomonas aeruginosa*. Popova *et al.* studied the antimicrobial effect of a cream containing extract of *P. sidoides* and colloidal nanosilver against *Escherichia coli*, *Staphylococcus aureus* and *Candida albicans* with significant antimicrobial activity.[11] The nanoformulation also presented effective healing *in vivo* on dogs with various skin diseases, demonstrating the cream's highly successful curative effect. As these works utilized the agar-gel disk diffusion method, only qualitative antimicrobial action could be evaluated.

Recurrent or persistent pulmonary infections that can significantly impair lung function and increase the risk of premature death and often involve opportunistic bacteria that colonize the respiratory tract, such as the Gram-positive *Staphylococcus aureus* and the Gram-negative *Pseudomonas aeruginosa*, *Klebsiella pneumoniae*, and *Escherichia coli*.[12] While research indicates that infections caused by *Staphylococcus aureus* and *Pseudomonas aeruginosa* are linked to more pronounced lung dysfunction in children.[13–15] *Pseudomonas aeruginosa* strains commonly cause pneumonia in older or immunodeficient patients, in the context of healthcare-associated infections, increasing morbidity and mortality in most cases[16] – in recent decades, this pathogen has been responsible for more than 20% of all hospital-acquired pneumonia cases worldwide, according to the Antimicrobial Surveillance Program SENTRY.[17] Typically found in the human intestinal microbiota, *Klebsiella pneumoniae* and *Escherichia coli* can also be detected in the oral microbiota, as well as in the urinary and nasal tracts of immunocompromised patients, hospitalized individuals undergoing invasive procedures, or those in intensive care units.[18] In cases of nosocomial and hospital-acquired infections, *Klebsiella pneumoniae* and *Escherichia coli* are frequently identified in instances of pneumonia.[19] In recent years, there has been a concern regarding multi-drug resistant bacteria. Among these pathogens, the carbapenemase-producing *K. pneumoniae* (KPC) is commonly known as a drug-resistant superbug/superbacterium, and its global dissemination and the restricted availability of treatment alternatives contribute significantly to its status as a prominent threat, mainly in terms of mortality. Besides, the few effective antibiotic therapies against KPC can give rise to severe adverse effects, such as nephrotoxicity and hepatotoxicity.[20,21] The development of new antibacterial compounds is highly necessary, as endorsed by global policies, such as those outlined by the World Health Organization.[22]

In this context, this study optimizes the synthesis of AgNPs through a green microwave-assisted procedure using the root extract of *P. sidoides*. In addition, using the broth microdilution method, we will assess the Minimum Inhibitory Concentration (MIC) of the crude *P. sidoides* extract and green-synthesized nanosilver to compare their antimicrobial activity against these important strains of pathogenic bacteria. Besides, the cytotoxicity of AgNPs was evaluated by a cell viability assay. To resume, we propose an antibacterial formulation based on green-synthesized AgNPs using *P. sidoides* extract to prospect alternatives and efficacious treatments to combat infections caused by multi resistant bacteria.

Experimental

Pelargonium sidoides extract

The plant extract used in this work – a commercial sample kindly provided by Centroflora Group (Brazil) – was obtained from roots of *Pelargonium sidoides* DC, of the family Geraniaceae, using extraction with water/ethanol and filtration techniques. The extract presents the following physicochemical characteristics: ethanolic extract (12.0% volume in CH_3CH_2OH) with a total solid content of a 0.60 ± 0.02% weight, pH = 6.5 ± 0.25 and density = 0.9798 ± 0.0004 g cm^{-1} (20 °C).

The phytochemical screening of the *P. sidoides* extract was performed using standard methods of prospection, and the following principal secondary metabolite groups were identified using this phytochemical analysis: alkaloids, anthocyanins, coumarins, flavonoids, phenols, saponins and tannins. Furthermore, the total polyphenol content was determined as 1.72 ± 0.015 mg mL^{-1} through the Folin–Ciocalteu method.[23]

Optimization of AgNPs synthesis

The microwave-assisted synthesis of AgNPs was performed in a Monowave 300 microwave reactor (Anton-Paar) using the mode "heat to temperature in time". In a typical procedure, the *P. sidoides* plant extract (PE) and $AgNO_3$ solution (1.0×10^{-3} mol L^{-1}) were mixed at a specific volume proportion (PE/$AgNO_3$ = 5, 10 or 15%) and the volume completed with water to 20.0 mL in a borosilicate glass vial. This solution was heated at constant power (800 W) at different temperatures (100, 150 and 200 °C) and times (5, 10 and 15 min), under magnetic agitation. After synthesis, 10 mL of acetone were added to induce precipitation, prior to the centrifugation of the obtained slurries. The supernatant was discarded, the excess acetone evaporated, and the precipitate was redispersed in water (pH ~ 7). Part of the sample was lyophilized for the characterization of AgNPs. All glassware and plasticware were sterilized before use. The suspension of AgNPs was filtered using a 0.25 μm PTFE syringe filter before characterization and biological tests.

Sample characterization

The following techniques were employed to characterize the synthesized samples: X-ray powder diffraction (XRD), with a Miniflex 600 Rigaku diffractometer operating at 40 kV, 30 mA and Cu-Kα radiation (λ = 1.541 Å); transmission electron

© 2024 The Author(s). Published by the Royal Society of Chemistry

Open Access Article. Published on 12 July 2024. Downloaded on 12/9/2025 5:59:04 AM.
This article is licensed under a Creative Commons Attribution-NonCommercial 3.0 Unported Licence.

microscopy (TEM), in a JEM-2100 JEOL microscope operating at 200 kV; Ultraviolet-visible spectroscopy (UV-vis), using a Hitachi 3900H spectrometer with a quartz cell (optical path = 1.0 cm); Fourier transform infrared spectroscopy (FTIR), in an IRPrestige-21(Shimadzu) spectrophotometer (resolution of 2 cm^{-1}) using KBr pellets in the region of 4000–400 cm^{-1}; X-ray photoelectron spectroscopy (XPS), in a SPECS SAGE HR 100 system spectrometer, with energy of 30 eV and 15 eV for analysis of the regions and of 285 eV for calibration of the binding energies of the peak C 1s. Zetametry and dynamic light scattering (DLS) were carried out using a Nano ZS ZetaSizer with MPT-2 Titrator (Malvern).

Evaluation of antibacterial activity

To study the antimicrobial activity of AgNPs, the minimum inhibitory concentration (MIC) and the minimum bactericidal concentration (MBC) of selected bacterial strains were determined using the broth microdilution method, according to the Clinical and Laboratory Standards Institute (CLSI).[24] The representative strains of the Gram-positive *Staphylococcus aureus* ATCC 29213 and the Gram-negative *Escherichia coli* ATCC 25922, *Pseudomonas aeruginosa* ATCC 27853 and the carbapenem-resistant *Klebsiella pneumoniae* ATCC BAA-1705 were grown in Müller-Hinton Broth (MHB) at 37 °C overnight. Serial dilutions of the nanoformulation containing AgNPs (0–1000 μg mL^{-1}) were made using a 96-well microdilution plate, resulting in approximately 1.5×10^4 CFU per well. The plates were incubated in a bacteriological oven at 37 °C for 24 hours and the procedure was performed in triplicate. Then, the absorbance of each well was read at 630 nm using a Multiskan microplate reader. Following incubation, bacterial inhibition was assessed by a change in color after the addition of the redox dye nitro-blue tetrazolium chloride (NBT). The lowest concentration that did not change the color of the dye was considered as the MIC against the target bacteria. All the experiments were performed in triplicate, and negative control was also included. The antimicrobial activity was also evaluated with pure extract of *Pelargonium sidoides* at the same experimental conditions.

Cell viability assay

A HaCat keratinocyte cell lineage of human origin was used to study the cytotoxicity of AgNPs. In a typical procedure, cells were kept in liquid nitrogen and, after thawing, acclimatized in a vial containing DMEM culture medium (Dulbecco modified Eagle's Minimal Essential Medium) supplemented with 1% antibiotic solution (penicillin and streptomycin) and 10% fetal bovine serum. The cells were kept in a humid incubator at 37 °C and 5% of CO_2 until reaching adequate confluence for the experiments, which were divided into the following groups: treated with pure *Pelargonium sidoides* extract (PE), with green synthesized nanostructures (AgNPs) and a negative control (without the formulation), at different concentrations. The treatments were performed in triplicate and cell viability was performed using the classical MTT (Methyl Thiazolyl Blue) assay,[25] to evaluate cellular metabolic activity. The quantification of cell viability was determined after reading the absorbance at 570 nm.

Statistical analysis

Data repeatability analyses were performed by calculating the Intraclass Correlation Interval at 95% and MIC and IC_{50} calculations through the methodology of adjustment to the response-sigmoidal dose curve. For these statistical analyses, SPSS software version 22.0 and GraphPad prism version 6.0 were used at a significance level of 5% ($p < 0.05$).

Results and discussion

Synthesis and sample characterization

Fig. 1a shows a typical X-ray diffractogram of AgNPs obtained using microwave-assisted green synthesis with *P. sidoides* extract. The main peaks with lattice planes $(111)_{Ag}$, $(200)_{Ag}$, $(220)_{Ag}$, and $(311)_{Ag}$ were identified and indexed for all samples

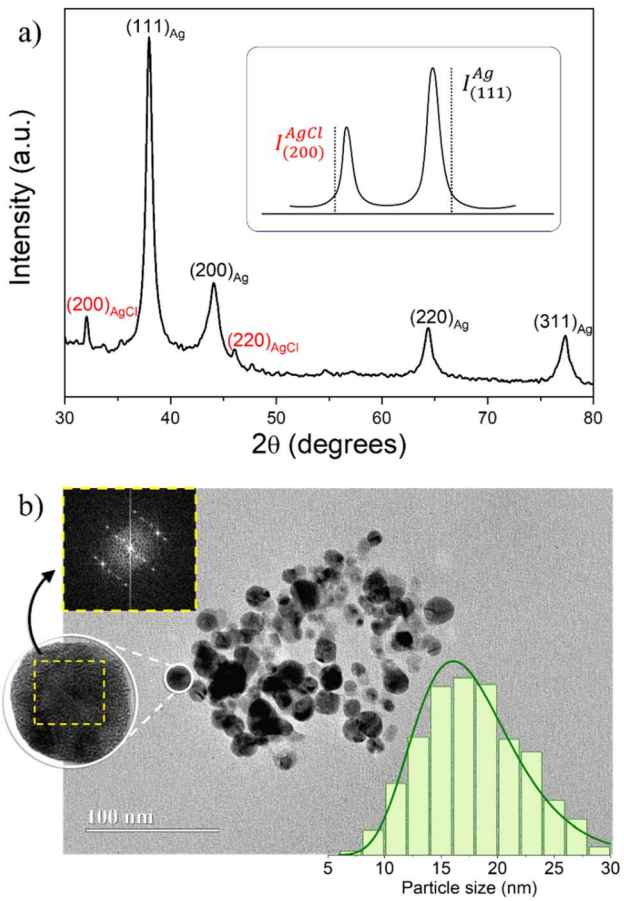

Fig. 1 XRD diffractogram (a) and TEM image (b) of AgNPs synthesized using PE/$AgNO_3$ = 10% at 200 °C for 15 min. The inset in (a) shows the relationship between the intensities of the most intense peaks of Ag^0 and AgCl phases ($I^{Ag}_{(111)}/I^{AgCl}_{(220)}$) used as a parameter to evaluate the yield of metallic AgNPs. The right-hand inset in (b) shows the size histogram and left-hand side inset shows a HRTEM image of a single nanoparticle (circle) and the corresponding FFT analysis (square).

Open Access Article. Published on 12 July 2024. Downloaded on 12/9/2025 5:59:04 AM. This article is licensed under a Creative Commons Attribution-NonCommercial 3.0 Unported Licence.

and correspond to the face-centered cubic (fcc) structure of metallic silver – Ag^0 (JCPDS #04-0783).

Besides, the extra peaks $(200)_{AgCl}$ and $(220)_{AgCl}$ were also detected in all diffractograms, indicating the formation of silver chloride, AgCl (JCPDS #31-1238), probably due to the spontaneous reaction of Ag^+ with Cl^- ions present in the plant extracts to form the very insoluble AgCl crystalline phase: $Ag^+_{(aq)} + Cl^-_{(aq)} \rightarrow AgCl(s)$; $K_{sp} \sim 10^{-10}$.[26] It was observed that the intensity of these peaks can be lower or higher depending on the synthesis conditions. Thus, we used the relationship between the intensities of the most intense peaks of Ag^0 and AgCl phases ($I^{Ag}_{(111)}/I^{AgCl}_{(220)}$) as a parameter to evaluate the yield of metallic AgNPs, in view of optimizing the synthesis conditions in the range of evaluated variables.[27]

A heat map with the values of $I^{Ag}_{(111)}/I^{AgCl}_{(220)}$ for all synthesized samples using the different combinations of plant extract and $AgNO_3$ volume proportion ($PE/AgNO_3$), temperature and time was used to compare the AgNP synthesis yield (Fig. 2). It was observed that increasing the temperature and the heating time enhanced the yield of metallic AgNPs during the synthesis process. Besides, the amount of AgNPs formed also increases as the $PE/AgNO_3$ rises from 5% to 10%, to a given temperature, indicating the effectiveness of the *Pelargonium sidoides* extract to reduce Ag^+ ions to form metallic AgNPs. However, if this $PE/AgNO_3$ ratio increases to 15% the quantity of AgCl rises while the Ag^0 formation diminishes.

Therefore, the sample synthesized using the optimized parameters $PE/AgNO_3 = 10\%$ at 200 °C for 15 min was characterized in detail and utilized for the further biological tests. As shown in a typical TEM micrography of the sample obtained using these conditions (see Fig. 1b), the AgNPs are roughly spherical, with a mean diameter of 17.1 ± 3.2 nm and polydispersity parameter equalling 0.26 ± 0.03, obtained from the lognormal fitting of the histogram (right-hand side inset of Fig. 1b). Besides, the crystalline size calculated using Scherrer's formula from the most intense XRD peak $(111)_{Ag}$ was ~14 nm, in good agreement with TEM size. The fast Fourier transform (FFT) analysis of the HRTEM single particle image (left-hand side inset of Fig. 1b) assessed its corresponding spot diffraction pattern, which matched the atomic planes of the cubic phase of metallic silver,[28] in good agreement with the XRD measurements.

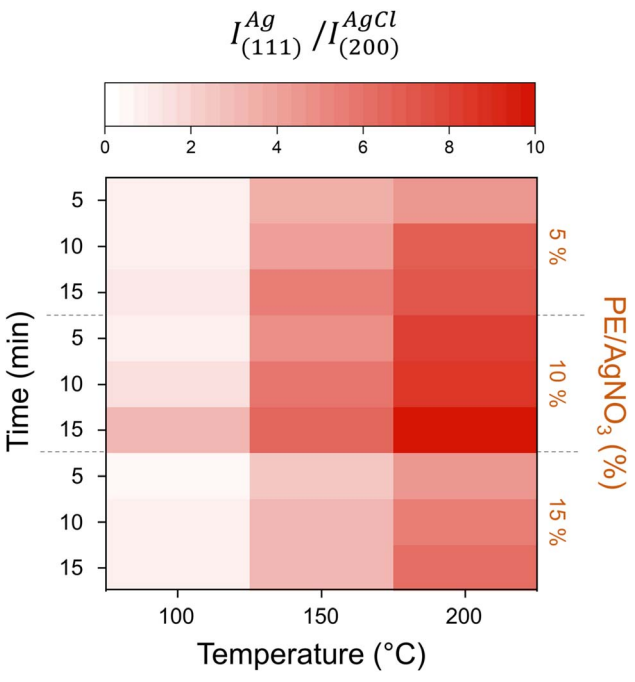

Fig. 2 Heat map with the AgNP synthesis yield ($I^{Ag}_{(111)}/I^{AgCl}_{(220)}$) at different times and $PE/AgNO_3$ as function of the temperature of synthesis.

The plant extract and the nanoformulation containing the AgNPs obtained using the optimized synthesis conditions were also characterized by UV-vis (Fig. 3a). The broad peak at the maximum wavelength of 436 nm in the UV-vis spectrum is due to the surface plasmon resonance of the AgNPs,[29] indicating the successful formation of nanosized structures from the microwave-green-mediated silver reduction ($Ag^+ \rightarrow Ag^0$). The broad absorbance before this plasmon resonance – also observed in the spectrum of the pure *P. sidoides* extract – has been attributed to the phytomolecules contained in the plant extract,[30] indicating a successful coating of AgNPs with these capping agents.

The FTIR spectrum of the AgNPs was obtained after separating the nanoparticles from the reaction medium by centrifugation, washing three times with ethanol/acetone, and lyophilizing overnight (see Fig. 3b). A summary of the wavenumbers and their corresponding tentative chemical assignments is provided in Table 1 for the crude plant extract and should be associated with the presence of its phytomolecules – coumarins and their methyl esters, flavonoids, tannins, phenols, *etc.* Particularly, the bands of the chemical moieties δ(N–H) and ν(C=O) at 1606 cm^{-1} and 1314 cm^{-1} have been identified as possible biomarkers characteristic of *Pelargonium sidoides* extract,[31] indicating a successful surface functionalization of silver nanoparticles with phytomolecules.

XPS was performed to probe the surface of the AgNPs synthesized with optimized conditions. The strong signals of O and C can be clearly observed, while the signal of silver is rather weak, in the XPS survey spectrum (see Fig. 4). This attenuation of the Ag 3d signal indicates that the surface of AgNPs is coated with organic molecules from the plant extract.

The high-resolution XPS Ag 3d core level spectrum of the synthesized sample shown in Fig. 4b is characterized by the presence of well-separated doublet peaks. This is due to the spin-orbital splitting of the components Ag $3d_{3/2}$ (367.6 eV) and Ag $3d_{5/2}$ (373.6 eV), confirming the successful formation of metallic nanosilver through the reduction of a silver salt by the plant extract.[35] Further, the Ag $3d_{5/2}$ peak was resolved into two different components, centered at 367.2 and 368.5 eV, which are attributed to Ag^0 and Ag^+ species, in good agreement with the results of XRD, which also indicate the formation of silver chloride besides the metallic nanosilver.

The high resolution XPS C 1s core-level spectrum in the range of 302–272 eV obtained from the AgNP sample (Fig. 4c) was deconvoluted into three peaks at 284.9 eV, 286.4 eV and 288.7 eV, which correspond to the binding energy of the C–C,

© 2024 The Author(s). Published by the Royal Society of Chemistry

Open Access Article. Published on 12 July 2024. Downloaded on 12/9/2025 5:59:04 AM.
This article is licensed under a Creative Commons Attribution-NonCommercial 3.0 Unported Licence.

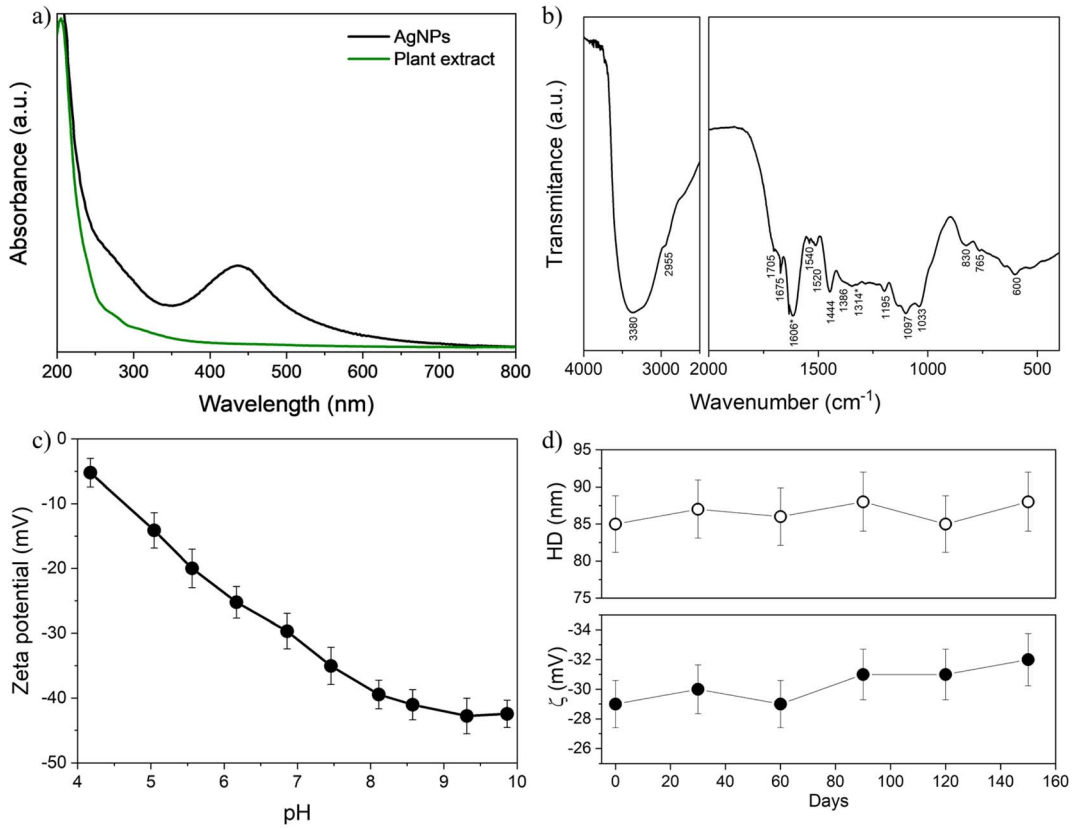

Fig. 3 UV-vis (a) and FTIR (b) spectra of nanosilver and plant extract. The FTIR bands marked with asterisk at 1606 cm^{-1} and 1314 cm^{-1} have been identified as possible biomarkers characteristic of *Pelargonium sidoides* extract.[31] (c) Zeta potential (ζ) as a function of the pH for AgNPs obtained using optimized synthesis. (d) Hydrodynamic size (HD) and zeta potential (ζ) of nanoparticles at pH ~7.

C–O and C=O moieties, respectively. The large peak in the O 1s core-level spectrum shown in Fig. 4d is ascribed to the convolution of the C–OH moiety in aliphatic and aromatic species, with components centered at about 532.5 and 533.5 eV, respectively. These results corroborate the analysis of FTIR, which shows the presence of moieties present in the phytomolecules of the *P. sidoides* extract.

Fig. 3c shows the variation of the zeta potential as a function of pH for the AgNPs synthesized with optimized conditions. The zeta potential of this sample, which is ~−5 mV at pH = 4, decreases as the pH of the dispersion rises to 10, up to −40 mV. This indicates the presence of ionizable anionic moieties, which undergo increasing deprotonation with pH on the surface of AgNPs.[36] At pH 7, in particular, the zeta potential module is higher than 30 mV at physiological pH, indicating high colloidal stability.[37] These observations also help confirm that the plant extract acts not only as a reducing agent to form the silver metallic core but as a capping agent to functionalize the

Table 1 Major vibrational bands (FTIR) and tentative assignments for investigated samples

Wavenumber (cm^{-1})	Assignments	Typical moieties
3380	ν(–OH)	Alcohols and phenols[10]
2955	ν(CH)	Alkanes[10]
2705	ν(CH)	Aldehydes[32]
1705, 1675	δ(C=O)	Carboxylic acid and esters[33]
1606	δ(N–H)	Amines[31]
1540, 1520	ν(NO)	Nitro compounds[34]
1444	ν(C=C)	Aromatic[33]
1386	δ(CH)	Alkanes[34]
1314	ν(C=O)	Aromatic esters[31]
1097	ν(C=O)	Esters and alcohols[33]
1033	ν(CN)	Aliphatic amines[34]
830	ν(CH)	Aromatic[10]
765–600	ν(C=C), δ(O–H)	Aromatic rings, phenolic bonds[10]

Open Access Article. Published on 12 July 2024. Downloaded on 12/9/2025 5:59:04 AM.
This article is licensed under a Creative Commons Attribution-NonCommercial 3.0 Unported Licence.

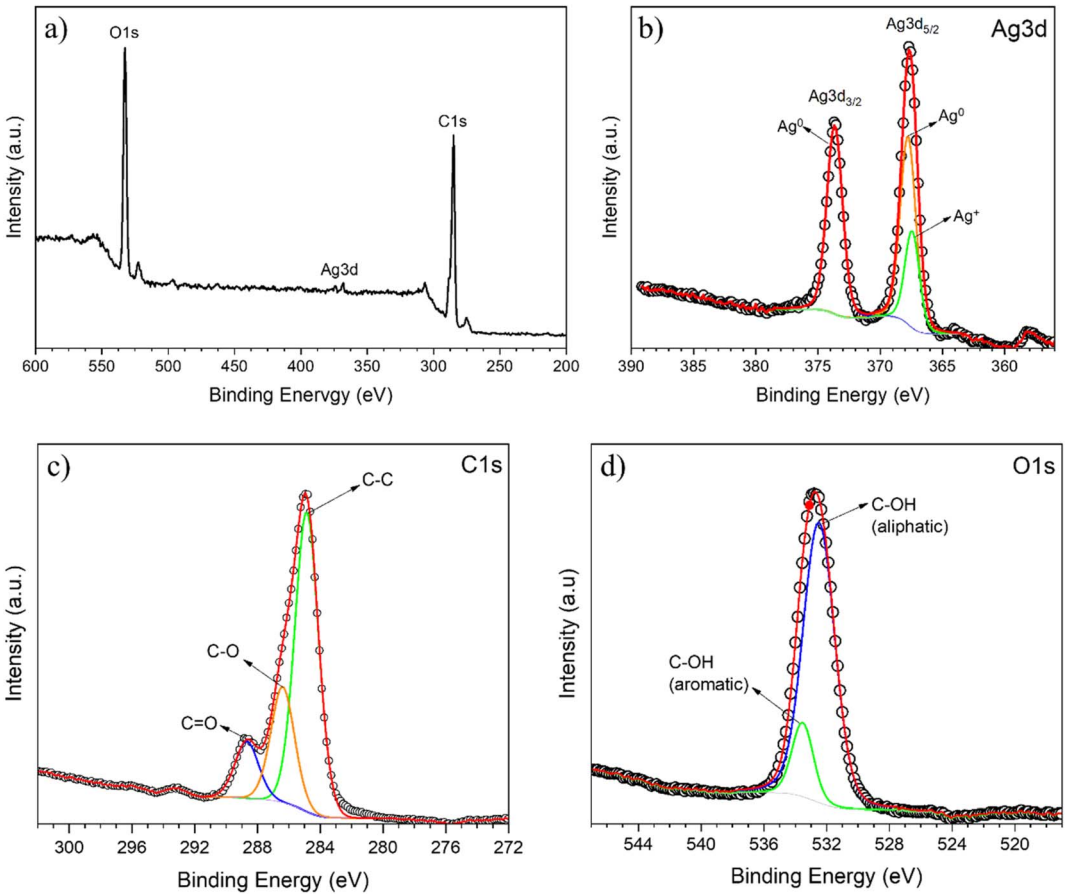

Fig. 4 XPS survey spectrum (a) and high resolution Ag 3d (b), C 1s (c) and O 1s (d) XPS spectra for AgNPs obtained using optimized synthesis.

surface of AgNPs with phytomolecules. Besides, as shown in the inset of Fig. 3c, at pH ~7 there were no significant variations in zeta potential (~−30 mV) and hydrodynamic size (~85 nm) as a function of the time for a diluted sol (stored in the dark) containing these AgNPs and investigated over 150 days. Along with the visual observations of no sedimentation, these results strongly suggest that the increased kinetic stability of the obtained colloids is achieved from electrosteric interparticle repulsion, due to ionizable moieties of the plant extract molecules adsorbed on the surface of metallic AgNPs.[27]

Biological tests

The antimicrobial activity of the nanoformulation with AgNPs was evaluated against representative strains of the widely used model bacteria *S. aureus* (Gram-positive) and *E. coli* (Gram-negative), along with the Gram-negative clinically important pathogens *P. aeruginosa* and the carbapenem-resistant superbug *K. pneumoniae* (KPC). The percentages of inhibition caused by the pure *P. sidoides* extract and the nanoformulation with AgNPs at different concentrations against these strains are shown in Fig. 5. It can be observed that the bacterial inhibition (*i.e.* the antibacterial activity) exhibited a dose–response dependence for both the pure extract and the nanoformulation containing the AgNPs, as their concentration increased from 50 to 1000 μg mL^{-1}, against all the studied strains. For the AgNP formulation against *K. pneumoniae*, this is less evident, as the antibacterial activity seems to be close to its maximum even at the lowest dose of the antimicrobials. In this case, no statistical difference was observed in the antibacterial activity as the concentration of the nanoformulation increased.

Overall, for all doses, the formulation with AgNPs displayed a larger antibacterial activity than the pure extract of *P. sidoides*, except in the case of *E. coli* at 50 μg mL^{-1}, which behaved in the opposite way. The largest difference was observed for *P. aeruginosa* at all concentrations, with emphasis on 50 μg mL^{-1} dose, where the bacterial activity of the nanoformulation was ~25 times higher than the activity of the pure plant extract. In particular, the observed antimicrobial effect of the AgNPs was higher against *P. aeruginosa* and *K. pneumoniae*, with inhibitions respectively exceeding 70% and approximately 100%, using only the lowest applied dose (50 μg mL^{-1}) of nanosilver.

Nevertheless, the mechanism of action of AgNPs has not been completely elucidated, and a prevailing theory suggests that free Ag^+ ions interact with bacterial membrane proteins, enhancing their permeability and culminating in cellular death.[38] In this instance, the Ag^+ species originate from the dissolution/desorption/oxidation of metallic silver (Ag^0) from the surface of AgNPs, which is contingent upon various parameters, such as inherent characteristics of silver

© 2024 The Author(s). Published by the Royal Society of Chemistry

Open Access Article. Published on 12 July 2024. Downloaded on 12/9/2025 5:59:04 AM.
This article is licensed under a Creative Commons Attribution-NonCommercial 3.0 Unported Licence.

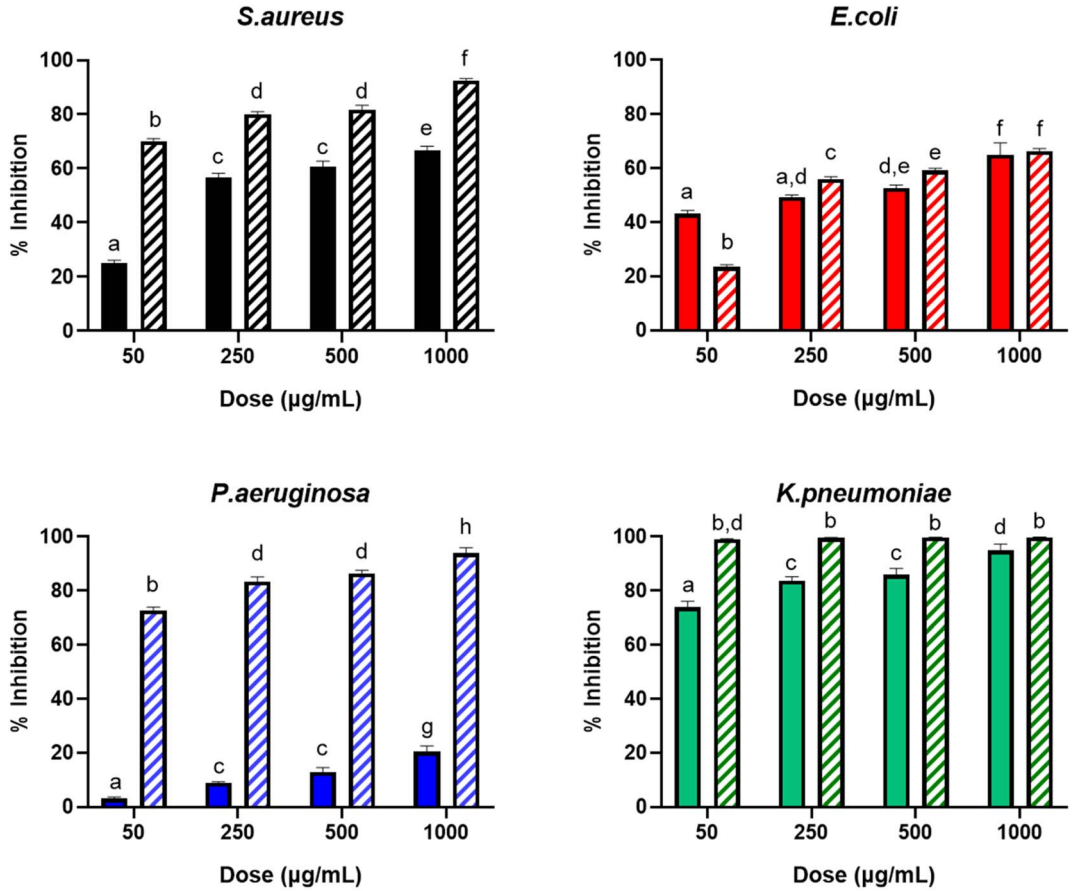

Fig. 5 Percentage of inhibition against different strains caused by pure extract of *P. sidoides* (filled bars) or nanoformulation containing green-synthesized AgNPs (hatched bars), at different concentrations. Data are presented as mean ± standard deviation. Different letters indicate statistically significant differences at $p < 0.05$.

nanoparticles and the surrounding environment. In this case, the size, shape, aggregation state, and presence of capping agents in AgNPs, as well as the ionic strength, presence of complexing agents, and pH of the medium, play a crucial role in this dissolution equilibrium.[39,40] Besides, because of their reduced size, AgNPs can anchor or penetrate cell walls, also causing membrane denaturation.[41] Thus, the layer of *P. sidoides* phytochemicals adsorbed on the surface of AgNPs is expected to influence this dissolution, in addition to possessing its own well-known biological activity against a variety of microorganisms.[42]

From the *in vitro* assays, the MIC and the MBC of the nanoformulation with AgNPs and the crude plant extract were calculated and listed in Table 2. In this work, the MIC indicates the lowest concentration needed to inhibit 50% of microbial growth and the MBC identifies the lowest concentration of the antimicrobial required to kill 99.9% of the bacterial inoculum. Results show that nanoformulation requires lower doses to inhibit bacteria when compared to the use of pure *P. sidoides* extract for all the investigated microorganisms, indicating a stronger inhibitory effect of nanosilver.

Green-synthesized nanosilver exhibited a potent antimicrobial efficacy against the top-listed bacteria that cause hospital-acquired infections, namely *S. aureus*, *E. coli* and *P. aeruginosa*. Besides, the nanoformulation containing the green-synthesized AgNPs presented surprisingly high efficiency against the carbapenemase-producing *K. pneumoniae*, in which a very low dose (MIC = 0.85 mg mL^{-1}) was needed to inhibit the growth of bacteria. It is important to emphasize that this is a highly pathogenic superbug, resistant to several known antibiotherapies, which has great significance for the public health, due to its widespread prevalence and consequential impact on factors such as mortality rates, quality of life, healthcare expenses, and potential for local and global transmission. The treatment of KPC using conventional drugs may result in profound adverse effects, notably including nephrotoxicity and hepatotoxicity.

Kgatshe *et al.*[10] showed silver nanoparticles obtained from *P. sidoides* extract also exhibited slightly larger antimicrobial activity compared to the plant extract against *Escherichia coli* (ATCC 25922) and *Pseudomonas aeruginosa* (ATCC 27853). However, only qualitative results were provided, since those researchers utilized the agar-gel disk diffusion method to determine the antimicrobial action. Other studies with quantitative data, such as MIC, were not found to compare with the results observed in our work.

Open Access Article. Published on 12 July 2024. Downloaded on 12/9/2025 5:59:04 AM. This article is licensed under a Creative Commons Attribution-NonCommercial 3.0 Unported Licence.

Table 2 Antibacterial activity of AgNPs against pathogenic bacteria

Strain	Formulation	MIC (μg mL^{-1})	Confidence interval (μg mL^{-1})	MBC ($\times 10^3$ μg mL^{-1})
S. aureus	PE	85.0	67–107	8.4
	AgNPs	12.0	6–25	1.1
E. coli	PE	267.0	192–373	26.4
	AgNPs	71.4	69–99	7.0
P. aeruginosa	PE	>10^3	—	—
	AgNPs	17.1	16–24	1.6
K. pneumoniae (KPC)	PE	21.1	13–35	2.0
	AgNPs	0.85	0.01–7.23	0.08

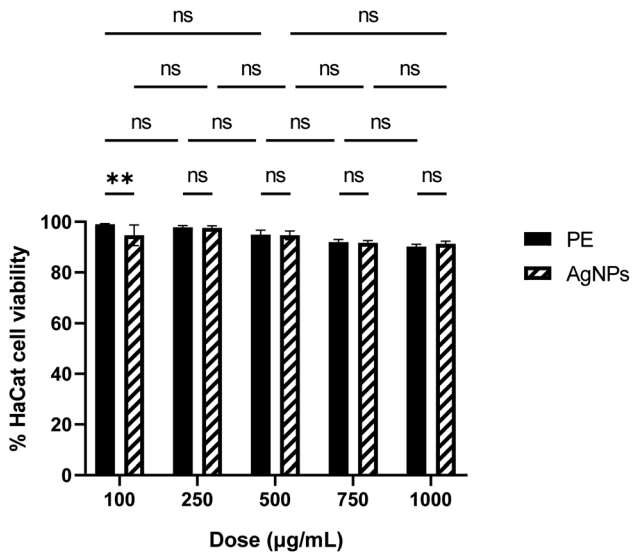

Fig. 6 Percentage of cell viability of HaCat in the presence of pure extract of *P. sidoides* (PE) or nanoformulation containing green-synthesized AgNPs. Data are presented as mean ± standard deviation and the asterisks indicate the statistical significance $^{**}p < 0.01$ and ns $p > 0.05$.

Fig. 6 depicts a viability plot profile for HaCat cells after treatment with *P. sidoides* extract and the nanoformulation containing AgNPs. Cell viability is very high, practically constant and no toxicity can be inferred from the data in the range of concentration investigated. Furthermore, there is no statistical distinction in cellular viability between treatments involving pure *P. sidoides* extract and the nanoformulation containing AgNPs at an equivalent antimicrobial concentration. The plant extract and AgNP formulations exhibited half-maximal drug inhibitory concentration (IC_{50}) values of 9.5×10^3 μg mL^{-1} and 10.3×10^3 μg mL^{-1}, respectively. Since the American National Cancer Institute (NCI) guidelines set the criteria of cytotoxicity activity for plant extracts IC_{50} less than 20 μg mL^{-1} as highly cytotoxic, our results show that the synthesized nanoformulation can be considered harmless to humans.[43]

Conclusion

In summary, microwave-assisted green synthesis employing *Pelargonium sidoides* DC roots extract has proven effective in producing silver nanoparticles (AgNPs) with desired structural and morphological characteristics. Optimization of synthesis parameters enhances the yield of AgNPs while maintaining particle integrity and ensuring reproducibility. Characterization techniques including XRD, UV-vis, FTIR and XPS confirm the successful synthesis and functionalization of AgNPs with organic molecules from the plant extract. Moreover, the observed colloidal stability underscores the versatility of this approach for nanomaterial production and highlights the promising role of natural extracts in nanoparticle synthesis and functionalization. The nanoformulation with AgNPs derived from *P. sidoides* extract demonstrates potent antimicrobial efficacy against a spectrum of pathogenic bacteria, including notorious drug-resistant strains such as carbapenemase-producing *K. pneumoniae* (KPC). The formulation exhibits a dose-dependent antibacterial activity, outperforming pure plant extract in most cases. The enhanced antimicrobial effect is attributed to the synergistic action of metallic AgNPs and phytochemicals from *P. sidoides*. Additionally, the nanoformulation shows promising biocompatibility, as evidenced by high cellular viability *in vitro*. These findings underscore the potential of green-synthesized nanosilver as a therapeutic agent against multidrug-resistant pathogens, warranting further exploration.

Data availability

All data (experimental procedures and characterization) that support the findings of this study are available within the article.

Conflicts of interest

The authors declare that there is no conflict of interest.

Acknowledgements

The authors express their gratitude for the financial support provided by the following Brazilian agencies: Fundação de Apoio à Pesquisa do Distrito Federal (FAPDF), Coordenação de Aperfeiçoamento de Pessoal de Nível Superior (CAPES) and Conselho Nacional de Desenvolvimento Científico e Tecnológico (CNPq). M. H. S. acknowledges FAPDF grant numbers 00193.00000767/2021-15, 00193-00001264/2021-67 and

 © 2024 The Author(s). Published by the Royal Society of Chemistry

Open Access Article. Published on 12 July 2024. Downloaded on 12/9/2025 5:59:04 AM. This article is licensed under a Creative Commons Attribution-NonCommercial 3.0 Unported Licence.

0193.00002588/2022-01, and CNPq grant number 315627/2021-2. The authors extend their appreciation to Dr Tatiane Oliveira dos Santos of the High-Resolution Microscopy Multi-User Laboratory at the Federal University of Goiás, Brazil, for conducting the electron microscopy measurements. The graphical abstract figure was created using the Microsoft Copilot artificial intelligence algorithm, for which we extend our gratitude. After using this tool, the authors reviewed and edited its content.

References

1 K. Kalantari, E. Mostafavi, A. M. Afifi, Z. Izadiyan, H. Jahangirian, R. Rafiee-Moghaddam and T. J. Webster, *Nanoscale*, 2020, **12**, 2268–2291.
2 Vidyasagar, R. R. Patel, S. K. Singh and M. Singh, *Mater. Adv.*, 2023, **4**, 1831–1849.
3 H. M. Fahmy, A. M. Mosleh, A. A. Elghany, E. Shams-Eldin, E. S. Abu Serea, S. A. Ali and A. E. Shalan, *RSC Adv.*, 2019, **9**, 20118–20136.
4 S. Simon, N. R. S. Sibuyi, A. O. Fadaka, S. Meyer, J. Josephs, M. O. Onani, M. Meyer and A. M. Madiehe, *Biomedicines*, 2022, **10**, 2792.
5 O. Kayser and H. Kolodziej, *Planta Med.*, 1997, **63**, 508–510.
6 D. Careddu and A. Pettenazzo, *Int. J. Gen. Med.*, 2018, **11**, 91–98.
7 O. Kayser, H. Kolodziej and A. F. Kiderlen, *Phytother. Res.*, 2001, **15**, 122–126.
8 M. Moyo and J. Van Staden, *J. Ethnopharmacol.*, 2014, **152**, 243–255.
9 H. Kolodziej, *Phytomedicine*, 2007, **14**, 9–17.
10 M. Kgatshe, O. S. Aremu, L. Katata-Seru and R. Gopane, *J. Nanomater.*, 2019, **2019**, 1–10.
11 T. P. Popova, I. Ignatov, T. E. Petrova, M. D. Kaleva, F. Huether and S. D. Karadzhov, *Cosmetics*, 2022, **9**, 122.
12 M. S. Niederman and D. E. Craven, *Am. J. Respir. Crit. Care Med.*, 2005, **171**, 388–416.
13 N. Pillarisetti, E. Williamson, B. Linnane, B. Skoric, C. F. Robertson, P. Robinson, J. Massie, G. L. Hall, P. Sly, S. Stick and S. Ranganathan, *Am. J. Respir. Crit. Care Med.*, 2011, **184**, 75–81.
14 D. J. Wolter, J. C. Emerson, S. McNamara, A. M. Buccat, X. Qin, E. Cochrane, L. S. Houston, G. B. Rogers, P. Marsh, K. Prehar, C. E. Pope, M. Blackledge, E. Déziel, K. D. Bruce, B. W. Ramsey, R. L. Gibson, J. L. Burns and L. R. Hoffman, *Clin. Infect. Dis.*, 2013, **57**, 384–391.
15 S. Malhotra, D. Hayes and D. J. Wozniak, *Clin. Microbiol. Rev.*, 2019, **32**, 138–184.
16 D. Reynolds and M. Kollef, *Drugs*, 2021, **81**, 2117–2131.
17 H. S. Sader, J. M. Streit, C. G. Carvalhaes, M. D. Huband, D. Shortridge, R. E. Mendes and M. Castanheira, *JAC Antimicrob. Resist.*, 2021, **3**, 1–7.
18 D. Chang, L. Sharma, C. S. Dela Cruz and D. Zhang, *Front. Microbiol.*, 2021, **12**, 1–9.
19 S. S. Jean, Y. C. Chang, W. C. Lin, W. Sen Lee, P. R. Hsueh and C. W. Hsu, *Jpn. Clin. Med.*, 2020, **9**, 275.
20 R. Podschun and U. Ullmann, *Clin. Microbiol. Rev.*, 1998, **11**, 589–603.
21 J. A. Ramos-Castañeda, A. Ruano-Ravina, R. Barbosa-Lorenzo, J. E. Paillier-Gonzalez, J. C. Saldaña-Campos, D. F. Salinas and E. V. Lemos-Luengas, *J. Infect.*, 2018, **76**, 438–448.
22 World Health Organization, *Prioritization of Pathogens to Guide Discovery Research and Development of New Antibiotics for Drug-Resistant Bacterial Infections, Including Tuberculosis*, Geneva, Switzerland, 2017.
23 A. J. Harborne, *Phytochemical Methods A Guide to Modern Techniques of Plant Analysis*, Springer, Dordrecht, 3rd edn, 1998.
24 Clinical and Laboratory Standards Institute (CSLI), *Methods for Dilution Antimicrobial Susceptibility Tests for Bacteria that Grow Aerobically*, Clinical and Laboratory Standards Institute, Wayne, PA, 11th edn, 2018, vol. 38.
25 S. Shrestha, P. Jiang, M. H. Sousa, P. C. Morais, Z. Mao and C. Gao, *J. Mater. Chem. B*, 2016, **4**, 245–256.
26 T. M. Pereira, V. L. P. Polez, M. H. Sousa and L. P. Silva, *Colloid Interface Sci. Commun.*, 2020, **34**, 100224.
27 R. P. Illanes Tormena, E. V. Rosa, B. de F. Oliveira Mota, J. A. Chaker, C. W. Fagg, D. O. Freire, P. M. Martins, I. C. Rodrigues da Silva and M. H. Sousa, *RSC Adv.*, 2020, **10**, 20676–20681.
28 L. C. Moraes, M. P. Gomes, R. Ribeiro-Andrade, Q. S. Garcia and C. C. Figueredo, *Environ. Pollut.*, 2023, **327**, 121483.
29 G. Z. S. Oliveira, C. A. P. Lopes, M. H. Sousa and L. P. Silva, *Int. Nano Lett.*, 2019, **9**, 109–117.
30 S. M. Yu, S. J. Kim, Y. C. Yoon and J. H. Kim, *J. Anal. Sci. Technol.*, 2021, **12**, 46.
31 J. E. Maree and A. M. Viljoen, *Vib. Spectrosc.*, 2011, **55**, 146–152.
32 M. Timotina, A. Aghajanyan, R. Schubert, K. Trchounian and L. Gabrielyan, *World J. Microbiol. Biotechnol.*, 2022, **38**, 196.
33 C. M. Topalăa and L. D. Tătarua, *Arab. J. Med. Aromat. Plants*, 2017, **3**, 1–9.
34 N. Konappa, A. C. Udayashankar, S. Krishnamurthy, C. K. Pradeep, S. Chowdappa and S. Jogaiah, *Sci. Rep.*, 2020, **10**, 16438.
35 R. B. Patil and A. D. Chougale, *Mater. Today: Proc.*, 2021, **47**, 5520–5532.
36 A. F. Palomec-Garfias, K. V. Jardim, M. H. Sousa and C. Márquez-Beltrán, *Colloids Surf., A*, 2018, **549**, 13–24.
37 S. Mourdikoudis, R. M. Pallares and N. T. K. Thanh, *Nanoscale*, 2018, **10**, 12871–12934.
38 M. P. Patil and G.-D. Kim, *Appl. Microbiol. Biotechnol.*, 2017, **101**, 79–92.
39 C. Ho, S. K. Yau, C. Lok, M. So and C. Che, *Chem.–Asian J.*, 2010, **5**, 285–293.
40 Z. Adamczyk, M. Oćwieja, H. Mrowiec, S. Walas and D. Lupa, *J. Colloid Interface Sci.*, 2016, **469**, 355–364.
41 C. Liao, Y. Li and S. Tjong, *Int. J. Mol. Sci.*, 2019, **20**, 449.
42 M. Moyo and J. Van Staden, *J. Ethnopharmacol.*, 2014, **152**, 243–255.
43 I. Canga, P. Vita, A. I. Oliveira, M. Á. Castro and C. Pinho, *Molecules*, 2022, **27**, 1–18.

© 2024 The Author(s). Published by the Royal Society of Chemistry